

Thermal decomposition behaviour and numerical fitting for the pyrolysis kinetics of 3D spongin-based scaffolds. The classic approach

Sonia Żółtowska^a, Iwona Koltsov^b, Krzysztof Alejski^a, Hermann Ehrlich^c, Michał Ciałkowski^d, Teofil Jesionowski^{a,*}

^a Poznan University of Technology, Faculty of Chemical Technology, Institute of Chemical Technology and Engineering, Berdychowo 4, 60965 Poznan, Poland

^b Laboratory of Nanostructures, Institute of High-Pressure Physics of the Polish Academy of Sciences, Sokolowska 29/37, 01142, Warsaw, Poland

^c TU Bergakademie Freiberg, Institute of Electronic and Sensor Materials, Gustav-Zeuner Str. 3, 09599 Freiberg, Germany

^d Poznan University of Technology, Faculty of Environmental Engineering and Energy, Institute of Thermal Engineering, Piotrowo 3, 60965 Poznan, Poland

ARTICLE INFO

Keywords:

Non-isothermal kinetics
Spongin
Pyrolysis
Thermogravimetric analysis

ABSTRACT

The kinetic parameters of thermal degradation of 3D skeletal biopolymer spongin - isolated from the marine demosponge *Hippospongia communis*, using thermogravimetric analysis (TG) were evaluated. The kinetic parameters of the pyrolysis in a nitrogen atmosphere were calculated using standard methods, including a model-fitting approach (Coats–Redfern method) and the model-free iso-conversional Friedman, Kissinger–Akahira–Sunose (KAS) and Ozawa–Flynn–Wall (OFW) methods. Based on the kinetic parameters obtained from the respective equations, the changes of entropy (ΔS), enthalpy (ΔH), and free Gibbs energy (ΔG) were evaluated using the theory of the active complex of the reagent. It was found that the chemical reaction model best describes the experimental data. The activation energies calculated by the Coats–Redfern method were in the range 39.3–48.7 kJ/mol. The calculated values of kinetics parameters are slightly lower than for the commercial polyurethane foams. Nevertheless, this study provides a comprehensive insight into the pathway, mechanism, and outcomes of pyrolysis of spongin-based scaffolds with the relation to the physicochemical characteristics of finally obtained carbon materials. Moreover, a critical discussion of the obtained results is given, with regard to the physical meaning of the applied approximations.

1. Introduction

The number of literature reports on carbon materials derived from biomass is constantly increasing. Most biopolymers (lignin [1,2], collagen [1,3,4], silk [5], cellulose [6], starch [6], chitin [6], keratin [7, 8]) as well as spongin [9,10] can be successfully used as precursors of carbon materials. Scientific efforts are currently directed towards the fabrication of fibrous-like carbon materials with ordered micro-structures, especially on a large scale [11,12] to produce the electrodes for supercapacitors, and catalysts support or carbocatalysts themselves. The high cost of obtaining carbon fibre materials is a limiting factor in their development, but also provides the main motivation to seek new and renewable structured precursors. Among the above-mentioned materials, spongin – a skeletal biopolymer of marine sponge origin – deserves special attention. Spongin, which belongs to the “collagen suprafamily” [9], is established as the main skeletal protein for constructing 3D skeletal formations exclusively in the Demospongiae

class of sponges; it is not found in any other organism in the animal kingdom [13]. The gross morphology and dimensions (up to 70 cm in diameter) of proteinaceous, spongin-based 3D skeletons have been known since ancient times in the form of commercial sponges [14]. Despite an annual market volume of more than US\$20 million, and extensive large-scale marine farming of these sponges worldwide, applications of sponges have been largely restricted to cosmetic uses [9].

It has recently been shown [9] that purified, mineral-free spongin can be converted to carbon at high temperatures without loss of its form or structural integrity, and that its specific surface area is increased due to the appearance of nanopores, favouring its further functionalization as a potential catalyst. Intriguingly, in contrast to the fragile carbonized scaffolds obtained from natural biomaterials by other groups (see Petrenko et al.), carbonized spongin remains stable enough to be sawn into slices up to 2 mm thick using a metallic saw with blade thicknesses of 1 mm. Nevertheless, spongin’s principal advantage in comparison with other foam-based materials [15–17] is related to the particular

* Corresponding author.

E-mail address: Teofil.Jesionowski@put.poznan.pl (T. Jesionowski).

<https://doi.org/10.1016/j.polymeresting.2021.107148>

Received 11 November 2020; Received in revised form 24 February 2021; Accepted 1 March 2021

Available online 4 March 2021

0142-9418/© 2021 The Author(s).

Published by Elsevier Ltd.

This is an open access article under the CC BY-NC-ND license

(<http://creativecommons.org/licenses/by-nc-nd/4.0/>).

hierarchical complex structure with nanofibres and triple helices of collagenous origin, which is preserved even after pyrolysis at temperatures as high as 1200 °C. Moreover, the chemical resistance of acid and enzymatic treatment and presence in its structure diverse heteroatoms might increase the diversity of surface functional groups and improve thermal stability. Likewise, their presence in the resulting carbon material structure can modify chemical reactivity and electrical conductivity, which is extremely important in designing new catalysts or electrode materials. However, the knowledge of thermal degradation kinetics is crucial to provide additional insight into the determination of optimal carbonization conditions.

Many recent papers describe the evaluation of the kinetic parameters of biopolymer pyrolysis using thermogravimetric analysis. Istrate et al. [18] evaluated the pyrolysis kinetics of hard α -keratin using the Friedman method and DSC measurements. The results indicate that activation energy decreases with an increase in the degree of conversion. These findings point to endothermic and irreversible reactions during pyrolysis. The calculated activation energy decreases from 135 kJ/mol for $\alpha = 0.3$ –93 kJ/mol for $\alpha = 0.9$. The authors clearly show that complex mechanisms are involved in the thermal degradation of α -keratin, and the pyrolysis occurs after damage to the keratin scaffolds. An investigation of the thermal degradation of collagen isolated from a mammal lens and rat tail was carried out by Miles et al. [19,20]. To evaluate the kinetic triplet the authors used calorimetric measurements, and the calculations were based on the Arrhenius equation. It was found that the origin of collagen influences the value of the activation energy. In the case of collagen from the mammal lens [19] the determined activation energy was 858 kJ/mol, but for the collagen from rat tails [20] the activation energy depended on the solvent used during calorimetric analysis: it was 521 kJ/mol for water and 1309 kJ/mol for acetic acid. The authors also indicate that the change of entropy for both tested origins of collagen has a positive value. These results are related to the cracking of α -chains and hydrogen bonds, which causes an increase in disorder during thermal treatment.

To the best of the authors' knowledge, the kinetics of the pyrolysis of spongin scaffolds isolated from demosponges have not been given great attention by researchers to date, and this fact motivated the present study. Therefore, the first part of the work aims to investigate experimentally the kinetics of thermal degradation of 3D spongin-based skeletal scaffolds of the *Hippospongia communis* marine sponge under different temperature programmes, using thermogravimetric analysis (TG). The kinetic parameters – activation energy E_A , pre-exponential factor A , and analytical form of reaction model function, $f(\alpha)$ or $g(\alpha)$ – were calculated using the Coats–Redfern method and by a model-free approach, including the KAS, OFW and Friedman methods. The evaluation of kinetic parameters is important from the process design point of view, to obtain a product with explicitly defined properties. Additionally, the information obtained from kinetic investigations is useful in determining the optimal conditions of pyrolysis: time of annealing, maximum temperature, and heating regime.

The studies about the kinetics of thermal degradation are fundamental from the designing point of view. Knowing the value of activation energy might be useful in determining and selecting of biomass precursor to the carbonization process. Moreover, combining this knowledge with the evaluation of received carbons' physicochemical properties will result in a comprehensive study regarding the pathway, mechanism, and outcomes of pyrolysis of particular biomass precursor. Consequently, the choice of proper material to prepare 3D, microporous, naturally structured bio-carbon for catalytic purposes could be justified. Presented results might be used as a reference point for the pyrolysis of various protein-based biopolymers.

2. Experimental part

2.1. Preparation of spongin

Marine demosponges of the species *Hippospongia communis* (Lamarck, 1814) were collected by scuba divers in the coastal waters of Tunisia in 2016, and were initially purified with distilled water to remove tissues and cells. The sponge skeletons prepared in this way, in the form of 3D scaffolds, were further sonicated for 5 h at 24 °C by experts from INTIB GmbH (Freiberg, Germany). In our laboratory, the obtained dry material was entirely immersed in 3 M HCl solution for 72 h at room temperature to remove residual calcium carbonates. Then the material was rinsed with distilled water until the pH of the solution reached 6.5, and was finally dried for 24 h at 50 °C in an oven (UF75 Memmert, Germany).

2.2. Thermogravimetric analysis

Thermogravimetric analysis (TG/DTG) (TG 209 Netzsch GmbH, Germany) was conducted to determine the degradation mechanisms and reaction kinetics. Measurements were carried out under flowing nitrogen (10 cm³/min) at heating rates of 2.5, 5, 10, and 20 °C/min over a temperature range of 25–1100 °C, with an initial sample weight of approximately 7 mg.

The volatile products released during heat treatment were identified with a mass spectrometer (QMS 403 Aëolos) coupled on-line to the TG/DTG instrument (STA 449 F1 Jupiter apparatus from Netzsch GmbH, Germany). The QMS was operated with an electron impact ionizer with an energy of 70 eV. The mass/charge (m/z) ratio was recorded in the range 2–100 AMU during the measurements. The TG/QMS analysis was performed under a continuous helium flow with initial sample mass equalled 20 mg. Obtained results were compared with the standard mass spectra of pure compounds found in the NIST database.

2.3. Characterization of the porosity of received carbon materials

To characterize the parameters of the porous structure of the biomaterials, surface area, total volume and an average size of pores were determined using an ASAP 2020 instrument (Micromeritics Instrument Co., USA). All samples were degassed at 120 °C for 24 h in a vacuum chamber before measurement. The surface area was determined by the multipoint BET (Brunauer–Emmett–Teller) method using adsorption data under relative pressure (p/p_0).

2.4. Kinetic study – theoretical background

The thermal degradation of spongin-based scaffolds as prepared was analysed using various methods. Data obtained from TG and DTG were used to determine the kinetic triplet: activation energy (E_A), pre-exponential factor (A), and reaction model $f(\alpha)$ [21–25]. The kinetic expression describing the temperature dependence of the rate constant can be written as follows:

$$r = \frac{d(m_a - m_f)}{dt} = k(T)f(m_a - m_f), \quad (1)$$

$$k(T) = A \exp\left(\frac{-E_A}{RT}\right), \quad (2)$$

where t denotes time (min), α is the degree of conversion, $f(m_a - m_f)$ is the kinetic part of the equation related to the mass of reactant taking part in the reaction, m_a and m_f are the masses of the sample measured for a

Table 1
Kinetic models used in solid-state reactions [27].

Chemical reaction	Model	$f(\alpha)$	$g(\alpha)$
1	N-power law	α^n	$\frac{1}{n-1} \left[\frac{1}{(1-\alpha)^{n-1}} - 1 \right]$
2	N^{th} order	$(1-\alpha)^n$	$\frac{1}{1-n} \alpha^{1-n}, n \neq 1$
Nucleation			
3	Avrami–Erofev A2	$2(1-\alpha)[- \ln(1-\alpha)]^{1/2}$	$[- \ln(1-\alpha)]^{1/2}$
4	Avrami–Erofev A3	$3(1-\alpha)[- \ln(1-\alpha)]^{2/3}$	$[- \ln(1-\alpha)]^{1/3}$
5	Avrami–Erofev A4	$4(1-\alpha)[- \ln(1-\alpha)]^{3/4}$	$[- \ln(1-\alpha)]^{1/4}$
Limiting surface reaction between both phases			
7	One dimension	1	α
8	Two dimensions	$2(1-\alpha)^{1/2}$	$1 - (1-\alpha)^{1/2}$
9	Three dimensions	$3(1-\alpha)^{2/3}$	$1 - (1-\alpha)^{1/3}$
Diffusion			
10	One-way transport	$1/2\alpha$	α^2
11	Two-way transport	$\frac{1}{\ln \frac{1}{1-\alpha}}$	$\alpha + (1-\alpha) \ln(1-\alpha)$
12	Three-way transport	$\left(\frac{2}{3} \right) (1-\alpha)^{2/3} \left[1 - (1-\alpha)^{1/3} \right]$	$\frac{9}{4} \left((1-\alpha)^{1/3} - 1 \right)^2$
13	Ginstling–Brounstein equation	$\left(\frac{2}{3} \right) (1-\alpha)^{1/3} \left[1 - (1-\alpha)^{2/3} \right]$	$\frac{9}{4} \left[- (1-\alpha)^{2/3} - \frac{3}{2} \alpha + 1 \right]$
14	Zhuravlev equation	$(1-\alpha)^{5/3} \left[1 - (1-\alpha)^{1/3} \right]$	$\frac{9}{4} \left[\frac{1}{(1-\alpha)^{1/3}} - 1 \right]^2$

specified α and in the final stage respectively, $k(T)$ is the kinetic rate constant, A (min^{-1}) is the pre-exponential factor, E_A (kJ/mol) is the activation energy, T is the absolute temperature, and R is the universal gas constant (8.314 J/mol.K).

The constant heating rate (β) may be defined as (3):

$$\beta = \frac{dT}{dt} = \text{constant} \quad (3)$$

$$dt = \frac{dT}{\beta} \quad (4)$$

On substituting $k(T)$ from equation (2) and dt from expression (4) into equation (1), and with some transformation, equation (1) can be written as:

$$\int_{\alpha_0}^{\alpha} \frac{d\alpha}{f(\alpha)} = \int_{T_0}^T A \exp\left(\frac{-E_A}{RT}\right) \frac{dT}{\beta} = g(\alpha). \quad (5)$$

To calculate the kinetic triplet it is essential to establish the conversion fraction, which is determined as the ratio of the current mass change to the total mass change (6):

$$\alpha = \frac{m_i - m_\alpha}{m_i}, \quad (6)$$

where m_b , m_f , and m_α are the initial, final, and current mass of the sample respectively.

2.4.1. Proposed approaches for calculations of the kinetic triplet

2.4.1.1. The model-fitting approach. Equation (5) may be solved using the approximation given by Coats and Redfern [26]. The obtained expression (7) is most frequently used to evaluate non-isothermal data and to calculate kinetic parameters:

$$\ln\left(\frac{g(\alpha)}{T^2}\right) = \ln\left(\frac{A R}{\beta E_A}\right) \left(1 - \frac{2RT}{E_A}\right) - \frac{E_A}{RT} \quad (7)$$

Since $2RT/E_A \ll 1$ the expression (7) may be simplified (8):

$$\ln\left(\frac{g(\alpha)}{T^2}\right) = \ln\left(\frac{A R}{\beta E_A}\right) - \frac{E_A}{RT} \quad (8)$$

The equations of the functions $f(\alpha)$ and $g(\alpha)$ depend on the pyrolysis mechanism and its mathematical model. The function $g(\alpha)$ usually represents the limiting stage of the reaction: chemical reaction, phase boundary reaction, random nucleation and nuclei growth, or diffusion. The application of the appropriate $g(\alpha)$ to the plot of $\ln[g(\alpha)/T^2]$ versus $1/T$ gives a straight line from which the values of E_A and A can be calculated. Table 1 shows the standard kinetic models and their algebraic expressions [22,27].

To check the correctness of the formulae presented in Table 1, the authors first determined the course of the function $T = f(\alpha)$ using a numerical method based on the equations given below (Table 1). It should be noted that the formulae in Table 1 have been modified by the authors to correspond to the relationship (9). The exact transformations can be found in the Supplementary Material:

$$g'(\alpha) = \frac{1}{f(\alpha)} \quad (9)$$

The kinetic parameters were calculated by the application of the appropriate $g(\alpha)$ to the plot of $\ln[g(\alpha)/T^2]$ versus $1/T$, from which the values of E_A and A can be calculated.

2.4.1.2. The iso-conversional approach. The Ozawa–Flynn–Wall method is based on Doyle's approximation of the temperature integral [21,28,29], which is (10):

$$p(x) = -2.315 + 0.457x, \quad (10)$$

where x means E_A/RT .

This approximation is inserted into equation (4), and after some rearrangement the final equation is obtained (11):

$$\ln(\beta) = \ln\left(\frac{A E_A}{R}\right) - 2.135 - 0.457 \frac{E_A}{RT} \quad (11)$$

The straight parallel line for the degree of conversion in the range

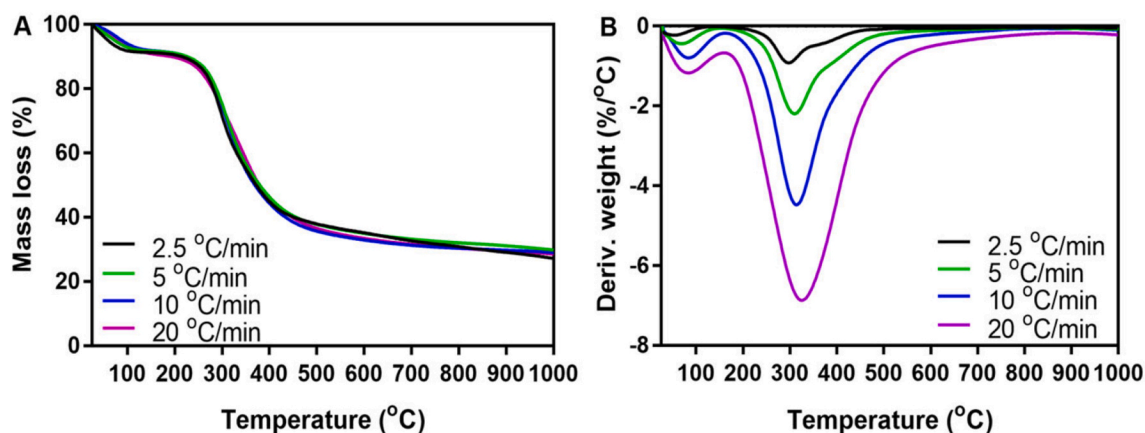


Fig. 1. TG (A) and DTG (B) curves for spongin-based scaffold, measured in the temperature range 25–1100 °C in a nitrogen atmosphere at different heating rates.

0–1 can be obtained by plotting $\ln(\beta)$ vs. $\frac{1}{T}$ at different heating rates and for each conversion, and then the E_A parameter can be calculated from the slope $0.457 \frac{E_A}{R}$.

The Kissinger–Akahira–Sunose (KAS) method is a model-free method based on the approximation $p(x) = x^{-2}e^{-x}$ [21]. The resulting equation is given below:

$$\ln\left(\frac{\beta}{T(\alpha)^2}\right) = \ln\left(\frac{AR}{E_A} + \ln[n(1-\alpha)^{n-1}]\right) - \frac{E_A}{RT(\alpha)}, \quad (12)$$

while the $T(\alpha)$ is the temperature measured for specified α . Then in the plot of $\ln\left(\frac{\beta}{T(\alpha)^2}\right)$ vs. $\frac{1}{T(\alpha)}$, the slope $-\frac{E_A}{R}$ gives the activation energy.

The Friedman method [30], also called the differential iso-conversional method, is based on equation (1) in the logarithmic form (13):

$$\frac{d\alpha}{dt} = \ln(Af(\alpha)) - \left(\frac{-E_A}{RT}\right) \quad (13)$$

The activation energy E_A for the specified value of the degree of conversion can be calculated from the slope of $\frac{d\alpha}{dt}$ vs. $\frac{1}{T}$. The Kissinger equation can be used to obtain the pre-exponential factor A (14):

$$A = \frac{\beta E_A}{RT_m^2} \exp\left(\frac{E_A}{RT_m}\right) \quad (14)$$

2.4.2. Thermodynamic study

The thermodynamic parameter can be derived from the fundamental expression of the theory of the active complex (15) [31]:

$$k = \frac{\chi e k_B T}{h} \exp\left(\frac{\Delta S}{R}\right) \exp\left(\frac{-E_A}{RT}\right), \quad (15)$$

where k_B is the Boltzmann constant, χ is a transmission coefficient which is unity for monomolecular reactions, h is the Planck constant, and ΔS is the change of entropy for the active complex.

Taking into consideration the pre-exponential factor from the Arrhenius equation (2), the expression (16) is obtained:

$$A = \frac{\chi e k_B T}{h} \exp\left(\frac{\Delta S}{R}\right) \quad (16)$$

After transformation of equation (16), the change of entropy of the active complex can be calculated from the following expression (17):

$$\Delta S = R \left(\ln A - \ln \frac{\chi e k_B T}{h} \right) \quad (17)$$

The changes of Gibbs free energy and enthalpy of the active complex

can be evaluated from well-known thermodynamic equations (18) and (19):

$$E_A = \Delta H + RT \quad (18)$$

$$\Delta G = \Delta H - T\Delta S \quad (19)$$

ΔS , ΔH , and ΔG are calculated at a temperature equal to the DTG peak temperature, which corresponds to the highest rate of the pyrolysis process.

Analysis and comparison of the calculated kinetic parameters enable the description of the process of thermal degradation of spongin.

3. Results and discussion

3.1. Thermogravimetric analysis of spongin-based scaffolds

The thermal degradation of spongin-based scaffolds was studied at four different heating rates (2.5, 5, 10, 20 °C/min) in the temperature range 25–1100 °C. Described approach was needed for kinetic parameters calculations. The TG and DTG curves obtained for different heating rates are presented in Fig. 1A and B, respectively. The data in Fig. 1A indicate that the heating rate does not influence the thermal degradation of the spongin material. There are two weight losses during thermal treatment. The first, a weight loss of approximately 10–12% in the range 80–150 °C, is related to the evaporation of physically absorbed and hydrogen-bonded water to the spongin skeleton [32,33]. The second, a 60–65% weight loss in the temperature range 200–420 °C, may be associated with the decomposition of the proteinaceous matrix: cracking of peptide bonds [32] and thermal degradation of disulphide bridges [32,34] and hydrogen bonds [32]. The negligible mass loss in the higher

Table 2

Possible product degradation identified by QMS during thermal treatment spongin scaffold in inert atmosphere.

Possible assignment	Characteristic peaks (m/z)
H ₂ O	16, 17, 18
CO ₂	12, 16, 22, 28, 29, 44, 45, 46
C ₂ H ₂	25, 26
C ₃ H ₆	27, 39, 40, 41, 42
(CH ₃) ₂ CO	43
NH ₃	15, 16, 17
NO	15, 16, 30
NO ₂	16, 30, 46
HCN	26, 27
CH ₃ CN	39, 40, 41
H ₂ S	33, 34
SO ₂	48, 64
(CH ₃ CO) ₂ S	43

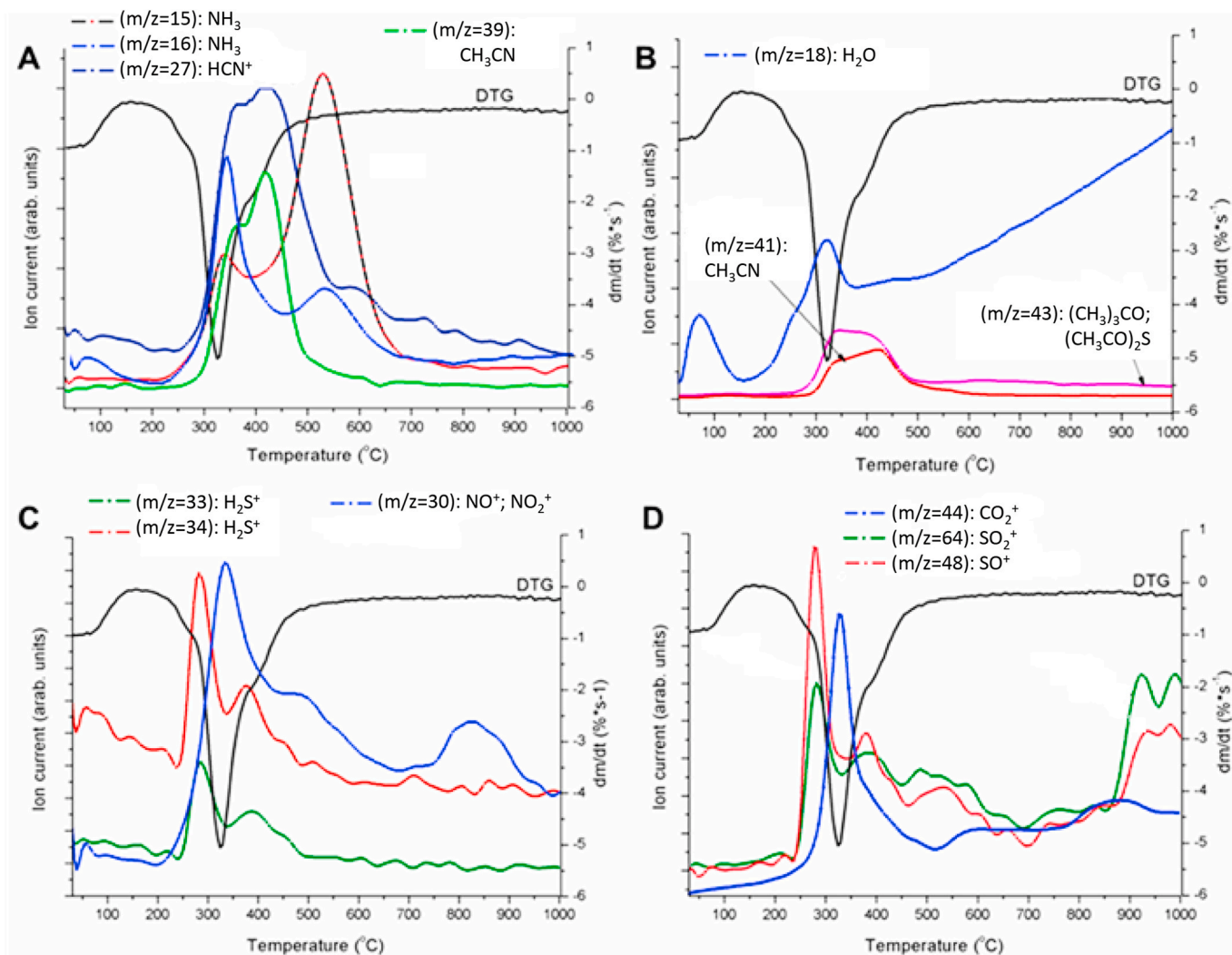


Fig. 2. DTG-QMS curves with examples of released gases during thermal treatment of spongin-based scaffolds.

temperature range could be associated with the different heating rates application, which affects the kinetics of material transformation.

From the data in Fig. 1B, it is apparent that the temperature of the DTG peaks is related to the heating rate: with an increase in the heating rate, the temperature at the DTG maximum (T_m) as well as the temperatures of the beginning and end of the process are shifted to higher values what is with the agreement to the common knowledge [35]. Consequently, the intensity of the DTG peaks on plots increases with the rising heating rate [11,21,35], which is also a very well-known phenomenon. The DTG curves collected with various heating rates were then used to calculate activation energy E_A and pre-exponential factor A , which is shown further in this work.

3.2. Analysis of volatile products using TG-QMS measurements

The qualitative analysis of released gases during thermal treatment was carried out using the quadrupole mass spectrometer (QMS 403C Aëolos) in the scan mode. The evolved gasses analysis of spongin-based scaffolds showed clearly the presence of simple gasses such as H_2O , CO_2 , NH_3 , NO , NO_2 , HCN , H_2S , SO_2 , as well as hydrocarbons: C_2H_2 , C_3H_6 , $(CH_3)_2CO$, CH_3CN (see Table 2). Table 2 contains only main, characteristic m/z signals used for peaks deconvolution. Fig. 2 presents DTG curves with chosen QMS signals collected during the thermal treatment of spongin-based scaffolds. For better understanding and quality of

Fig. 2, the authors decided not to show all recorded m/z lines.

Based on Fig. 2 and Table 2, it can be seen that the first mass loss during thermal treatment is related to the evaporation of water adsorbed onto the spongin skeleton at a temperature near 100 °C. At higher temperatures, the evolution of humidity presents a peak at 300 °C. Short-chain alkenes such as C_2H_2 and C_3H_6 are formed at 200–700 °C, with broad evolution peaks. In this temperature range, the evolution of $(CH_3)_2CO$ was also observed. The carbon matrix's degradation via CO_2 release from ~200 to 500 °C (at 340 °C a sharp peak with m/z 44 can be observed. Small peaks at ~600 °C and 890 °C are also visible, which may be related to the carbon chains' slow pyrolysis. The release of sulphur dioxide is a multi-step process (the $m/z = 48$ is characteristic for SO^+ , and $m/z = 64$ is assigned to SO_2^+). There are two distinctive regions. The first region with the highest intensity of peak at 270 °C and the second region of further SO_2 release occurs at a temperature range from 890 to above 1000 °C in two stages. Moreover, the presence of H_2S was observed in the temperatures range of 250–450 °C. The nitrogen-rich compounds have also been released in a multi-step process. Ammonia appears in two stages at a temperature range of 250–700 °C. The formation of HCN has been proved and occurred at temperatures between 250 and 600 °C. Release of NO and NO_2 was observed in two temperature ranges: 200–500 °C and 600–950 °C. The presence of CH_3CN in the was detected at the temperature range from 280 to 500 °C.

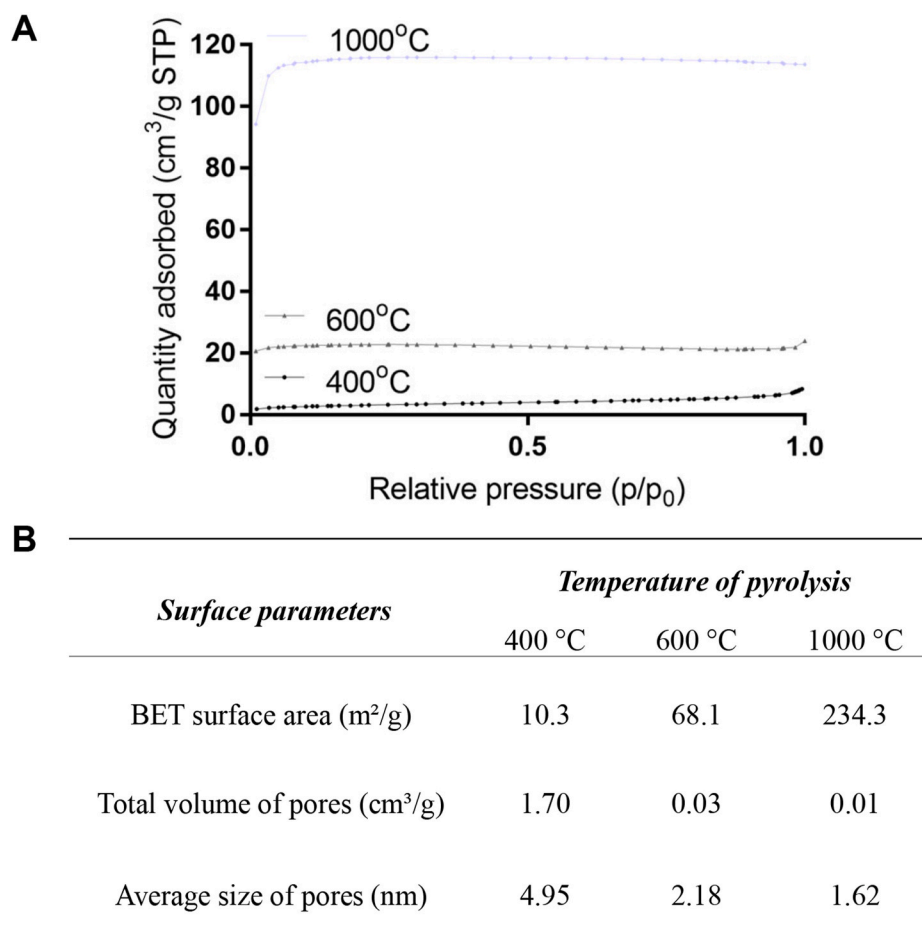


Fig. 3. The BET isotherms plots (A) with the tabular representation of the surface properties (B).

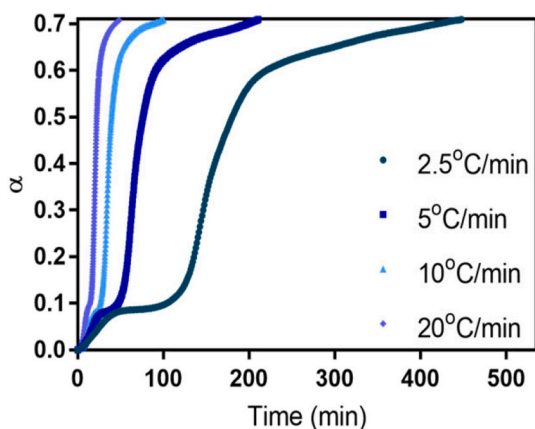


Fig. 4. Reaction profiles of spongin pyrolysis for different heating rates.

3.3. The determination of the influence of pyrolysis temperature on porous structure parameters of resulted materials

The low-temperature nitrogen sorption tests have been carried out for materials obtained after pyrolysis at 400, 600 and 1000 °C to investigate the effect of pyrolysis temperature on the porosity of resulted carbon-based materials. These temperatures were chosen based on the TG-QMS measurements. The obtained results are shown in Fig. 3.

Spongin-based scaffolds as a heterogeneous material derived from nature had estimated surface area in the range of 3.4 m²/g [9]. Consequently, the spongin-based precursor's thermal pyrolysis led to the

increased surface area, moreover, when the pyrolysis temperature increases, the BET surface also increases. However, opposite correlations are observed for the values of pore volumes and average pore sizes which decrease with the increases of pyrolysis temperature. According to the literature, a further increase in pyrolysis temperature led to turbostratic disordered carbon formation with microporous structure [9]. From the data presented above, it can be seen that the increase in the temperature of heat treatment enhances the skeletal structure of the resulted carbon-based materials.

3.4. Kinetic study

3.4.1. Determination of kinetic parameters by the Coats–Redfern approach

The Coats–Redfern approach assumes the application of various kinetic models to express the dependence of conversion on the process rate (for details, see Table 1). However, it must be pointed out that all of the models presented in Table 1 are specific only for solid-state reactions. Despite the significant number of reaction models, they can be divided into four main groups: chemical reactions, nucleation and growth of nuclei, limiting surface reaction between two phases, and diffusion models. Each group is associated with a specific shape of the plot showing changes in the extent of conversion (α) over time. The experimental data were plotted to obtain a reaction profile (as shown in Fig. 4) to choose the most reliable kinetic model.

In the reaction profiles presented in Fig. 3, several stages can be differentiated. First, the initial, small, and rapid evolution of gases (for the α range 0.0–0.11) may be identified as the decomposition of some impurities and evaporation of physically adsorbed water. This small input is omitted from the overall kinetic calculations [27]. Second, for α

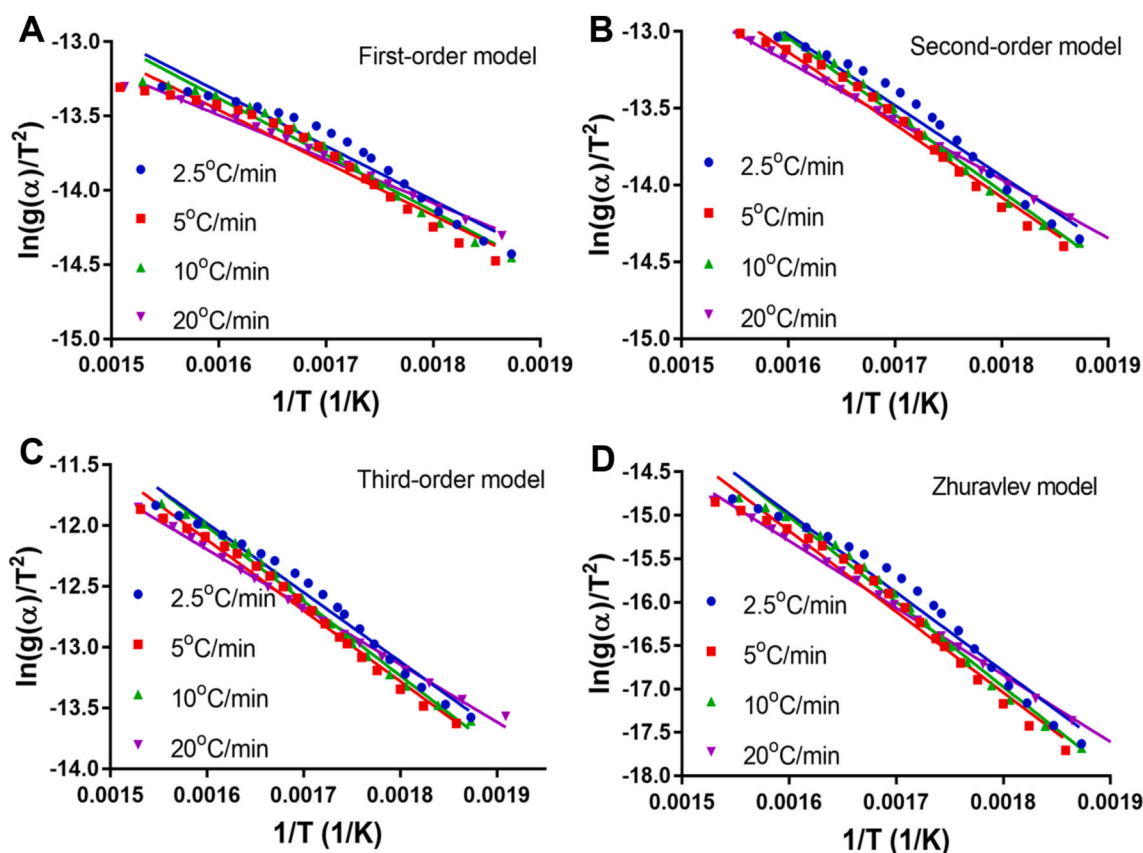


Fig. 5. First-order (A), second-order (B), third-order (C) and Zhuravlev (D) models evaluated for the experimental data.

Table 3

Kinetic triplet calculated from first-, second- and third-order models and the Zhuravlev model.

First-order model			
β ($^{\circ}\text{C}/\text{min}$)	E_A (kJ/mol)	$\ln A$ (min^{-1})	r^2
2.5	30.36	0.004	0.943
5	29.49	0.003	0.947
10	31.63	0.005	0.971
20	24.59	0.001	0.994
Second-order model			
2.5	38.29	0.032	0.965
5	39.28	0.036	0.976
10	41.55	0.064	0.989
20	31.77	0.006	0.997
Third-order model			
2.5	47.23	0.298	0.978
5	48.35	0.382	0.986
10	48.70	0.817	0.993
20	39.32	0.092	0.999
Diffusion model 4 – Zhuravlev equation			
2.5	75.54	11.691	0.964
5	77.43	1.159	0.975
10	81.47	15.335	0.988
20	64.15	0.809	0.988

higher than 0.11, the primary pyrolysis process begins, this having the highest rate. The observed bed of the curve is a consequence of the linear increase in temperature, which enhances the kinetics of decomposition; however, the amount of reactant decreases.

Interestingly, a plateau in the course of the degradation process over time is observed with increasing heating rate – this induction period may be related to the slow process of reaching equilibrium with the external furnace temperature. The possibility of formation of active nucleation species must be discounted due to the organic nature of spongin. Next,

the rate of decomposition progressively increases in the acceleration period to reach the maximum rate. Then the deceleration period begins, lasting until the reaction is completed.

Data obtained from the thermogravimetric analysis were applied for the determination of kinetic triplets using the proposed models (Table 1). The highest correlation coefficient was achieved for the reaction model and diffusion model type 4 – the Zhuravlev equation – as shown in Fig. 5. The calculated activation energies and pre-exponential factors are shown in Table 3.

Linear correlation of the experimental data was achieved for values of α in the range 0.2–0.5, and the calculations were carried out for this range. Based on the calculations, the third-order model has the highest correlation coefficient, and this model seems to define the mechanism of thermal decomposition with the greatest accuracy (for comparison, see Table 3).

It is visible that the activation energy varies with increasing heating rate, reaching the highest value for $\beta = 10$ $^{\circ}\text{C}/\text{min}$ and the lowest for $\beta = 20$ $^{\circ}\text{C}/\text{min}$. This behaviour may be explained by the fact that with increasing heating rate, the rapid pyrolysis of organic matter is observed, as was confirmed in the DTG analysis (see Fig. 1B). Similarly, the value of the correlation coefficient increases with increasing heating rate, independently of the applied reaction model – reaching the value 0.999 for the third-order model. This finding suggests that at the highest heating rate, the thermal decomposition of spongin-based scaffolds exhibits the least deviations, and therefore the experimental data can be fitted to the model. Based on the data in Table 3, the third-order reaction model was found to be appropriate to approximate the mechanism of thermal degradation.

It should be noted that for the Zhuravlev model, the calculated E_A values are significantly higher than for the other models. On the other hand, for this model, the correlation coefficients were not the highest. Nevertheless, it must be mentioned that such correlation of

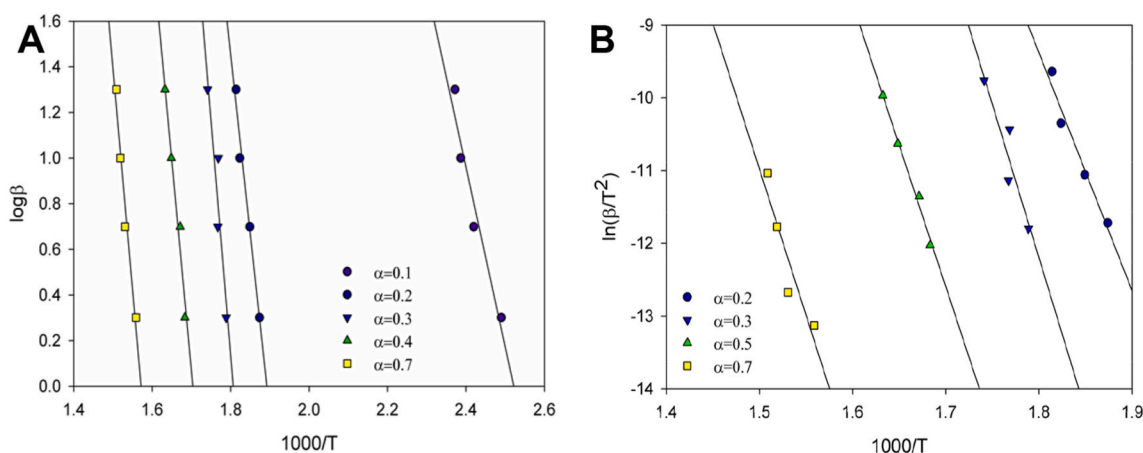


Fig. 6. OFW (A) and KAS (B) models obtained for the thermal degradation of spongin scaffolds.

Table 4

Arrhenius parameters and regression factors for the thermal degradation of spongin scaffolds according to the OFW method.

OFW			
A	E_A (kJ/mol)	A (min^{-1})	r^2
0.1	143.39	0.00063	0.940
0.2	286.25	0.001889	0.978
0.3	374.63	0.004248	0.881
0.5	336.42	0.005982	0.969
0.7	353.01	0.009028	0.964
KAS			
A	E_A (kJ/mol)	A (min^{-1})	r^2
0.2	272.24	$3.34 \cdot 10^{23}$	0.763
0.3	350.41	$4.47 \cdot 10^{27}$	0.872
0.5	323.27	$1.73 \cdot 10^{23}$	0.989
0.7	333.78	$2.44 \cdot 10^{21}$	0.866

experimental data with the Zhuravlev model may lead to false findings concerning the mechanism of thermal decomposition. During spongin pyrolysis, diffusion has little influence on the process kinetics. A similar situation is observed for the nucleation and nuclei growth mechanism: due to the protein nature of spongin-based scaffolds, the growth of nuclei is a negligible process in the overall pyrolysis.

3.4.2. Iso-conversional methods

The information obtained from TG was applied in calculations using the iso-conversional method according to the OFW and KAS models. The obtained regression lines are shown in Fig. 6A and B, respectively.

It should be noted that these methods do not take into consideration the reaction order and degradation mechanism. The calculated values of E_A and A from the OFW and KAS models are summarized in Table 4.

It can be seen from the data in Table 4 that the values of activation energies vary with the extent of conversion α . For $\alpha = 0.2$, an abrupt increase from 143.39 to 286.25 kJ/mol in the value of E_A can be observed. The result suggests that for the decomposition of fibres and breaking of the disulphide bridges and peptide bonds of spongin-based scaffolds, a higher activation energy is required [32,34]. Above $\alpha = 0.5$, minor fluctuations in the values of calculated activation energy are observed. This fact may be related to the further decomposition of proteinaceous scaffolds [33]. The results also show that the regression coefficients are lower than in the case of the Coats–Redfern method (see Table 3), which means that the OFW model is less well correlated with the experimental data.

The activation energy of the spongin-based scaffold's thermal degradation was also calculated using the KAS method (Fig. 6B). The

kinetic parameters were evaluated from the slope and intercept of the obtained equation (12). E_A values differ with degree of conversion, the lowest value was calculated for $\alpha = 0.2$, and others vary in the range of 323–350 kJ/mol. Interestingly, the values of the pre-exponential factors are significantly higher than those calculated using the OFW approach. Moreover, it is notable that the correlation coefficients (r^2) have smaller values than other methods (Coats–Redfern and OFW). Nevertheless, the activation energy calculations were also carried out using the KAS approach with the simplification and narrowing of the temperature range that corresponded to the highest process velocity. This is shown in the Supplementary Material.

Calculations of the kinetic triplet were also carried out using the Friedman method. However, because of the low correlation coefficient obtained, this method was not taken into further consideration. For more details, see the Supplementary Material.

The most striking result to emerge from these data is the fact that the calculated activation energies from the OFW method are significantly higher than those obtained from the Coats–Redfern and KAS methods. These results may be related to the different approximations used in each method. These relations are correct if the extent of conversion does not influence the activation parameters. Thus, if the activation parameters are dependent on the extent of conversion, these derivations are not appropriate. Therefore, in such cases, the Coats–Redfern method, which uses the reaction rate equation directly, is recommended.

The methods proposed in this work are commonly applied in the determination of kinetic parameters of inorganic compounds as well as various biomaterials, as described in the introduction. Therefore, at present such methods are assumed to be valid when discussing the mechanism of thermal decomposition and comparing the values of kinetic parameters for various materials. Nevertheless, they suffer from various drawbacks. For example, the solid-state reaction models were derived for simple inorganic compounds. Therefore, their use to describe the thermal degradation kinetics of biopolymers can often lead to good data correlation and thus a high correlation coefficient, but the assumed decomposition mechanism will be significantly simplified.

On the other hand, the model-free methods seem to overcome the problem of simplification of the mechanism. They are based on approximation of the temperature integral and work only in the region of linear temperature change. Moreover, these techniques can be applied only if the extent of conversion does not influence the kinetic parameters, which is not always the case for biopolymers. However, the proper approximation of the temperature integral is also not yet established [36]. Therefore, the iso-conversional methods may also lead to errors in activation energy evaluation. Consequently, the development of a new method to investigate kinetic parameters may solve some of the problems of the currently existing pathways.

It may be noted, however, that most studies have concerned

Table 5
Thermodynamic parameters of thermal degradation of spongin-based scaffolds.

Model	β	ΔS	ΔH	ΔG
	$^{\circ}\text{C}/\text{min}$	$\text{J}/\text{mol}\cdot\text{K}$	kJ/mol	kJ/mol
Third-order model	2.5	-323.65	94.53	278.66
	5	-266.77	96.63	251.53
	10	-260.53	97.45	250.20
	20	-278.86	89.12	256.14

calculation of the kinetic parameters of thermal degradation of well-studied biopolymers: chitin, lignin, cellulose, wood fibres, and others [37–39]. Few of them are focused on determination of the activation energy of the thermal degradation of collagen or keratin. Gil et al. [40] concluded that the thermal degradation of collagenous wastes occurs in three stages, and the activation energy of each step varies between 63 and 179 kJ/mol. Also important is the finding that spongin is structurally close to collagen, although its thermal degradation takes a different course. Thus, it is difficult to relate to these results directly. Independently of the model applied, the results are consistent with the activation energies evaluated for the thermal degradation of proteins. According to Bischof et al. [41] and Istrate et al. [18], pyrolysis of proteins is characterized by a wide range of activation energies, and these are generally related to the amino acid composition.

On the other hand, comparing values calculated for spongin-based scaffolds with data obtained for the polyurethane foams, the latter is characterized by higher activation energies than those calculated for spongin-based scaffolds [42,43]. However, spongin-based scaffolds' thermal stability slightly lower, reaching approximately 140 $^{\circ}\text{C}$, while for polyurethane foams it lies in the range of 200–300 $^{\circ}\text{C}$. Nevertheless, due to its superior physicochemical and morphological properties, spongin-based scaffolds seem to be a promising source for preparing structured microporous bio-carbons. Moreover, due to global contamination of the world ocean with micro- and nano-plastics, studies on naturally pre-structured and ready to use selected biodegradable biopolymer-based 3-D constructs are in trend now.

3.3.4. Thermodynamic calculations

To gain an accurate understanding of the mechanism of thermal decomposition of the studied spongin-based scaffolds, the changes of entropy (ΔS), Gibbs free energy (ΔG) and enthalpy (ΔH) were calculated. The values obtained are summarized in Table 5.

The negative value of ΔS suggests a reduction of random effects at the gas-solid interface and a decrease in the degree of freedom of the substances during the thermal decomposition process. Positive values of ΔG confirm that degradation is a forced process. It should be noted that for the rate $\beta = 20$ $^{\circ}\text{C}/\text{min}$, independently of the model applied, the ΔH value is lower than in the case of other heating rates. This finding confirms the fact that with an increase in heating rate, the energy required for thermal decomposition of spongin-based scaffolds is lower.

4. Conclusion

Knowledge of pyrolysis's kinetics is extremely useful in determining the optimal conditions for the carbonization on any material with the potential to be applied in material science. Due to the superior properties of spongin-based scaffolds isolated from *H. communis* sponge skeletons in preparation of microporous, hierarchical carbonaceous materials, this work focused on evaluating the kinetics parameters of its thermal degradation process. The TG analysis revealed that this biomaterial's thermal degradation does not depend on the heating regime, and during pyrolysis, two weight losses can be observed. The kinetic parameters were calculated using the Coats–Redfern, OFW and KAS methods. The obtained activation energies from the Coats–Redfern method were in the range 39.3–48.7 kJ/mol. However, high correlation coefficients with the experimental data were also obtained for the solid-

state reaction Zhuravlev model, with calculated activation energies in the range 64.2–81.5 kJ/mol. This work provides a comprehensive analysis of the pyrolysis of spongin-based scaffolds, with the evaluation of the most popular methods of calculation.

CRedit authorship contribution statement

Sonia Żóltowska: Conceptualization, Investigation, Writing – original draft, Writing – review & editing. **Iwona Koltsov:** Investigation. **Krzysztof Alejski:** Formal analysis, Writing – review & editing. **Hermann Ehrlich:** Writing – review & editing. **Michał Ciałkowski:** Formal analysis, Writing – review & editing. **Teofil Jesionowski:** Supervision, Writing – review & editing, Funding acquisition.

Declaration of competing interest

The authors declare that they have no known competing financial interests or personal relationships that could have appeared to influence the work reported in this paper.

Acknowledgements

The work was supported by the National Science Centre, Poland, project Etiuda no. 2019/32/T/ST8/00414. HE was supported by a Polish Honourable Alexander von Humboldt Fellowship (FNP, Poland). The authors would like to thank Marcin Wysokowski, Ph.D., of Poznan University of Technology for his help during the preparation of this manuscript as well as Katarzyna Siwińska-Ciesielczyk D.Sc., Ph.D., of Poznan University of Technology, for her assistance in nitrogen low-temperature sorption measurements.

Appendix A. Supplementary data

Supplementary data to this article can be found online at <https://doi.org/10.1016/j.polymertesting.2021.107148>.

References

- [1] Z. Zhao, F.S. Cannon, C. Nieto-Delgado, L. Pena, Lignin/collagen hybrid biomaterials as binder substitute for specialty graphites and electrodes, *Carbon* 108 (2016) 303–317, <https://doi.org/10.1016/j.carbon.2016.07.026>.
- [2] W. Qu, Y. Xue, Y. Gao, M. Rover, X. Bai, Repolymerization of pyrolytic lignin for producing carbon fiber with improved properties, *Biomass Bioenergy* 95 (2016) 19–26, <https://doi.org/10.1016/j.biombioe.2016.09.013>.
- [3] Y.H. Lee, F. Li, K.H. Chang, C.C. Hu, T. Ohsaka, Novel synthesis of N-doped porous carbons from collagen for electrocatalytic production of H_2O_2 , *Appl. Catal. B Environ.* 126 (2012) 208–214, <https://doi.org/10.1016/j.apcatb.2012.06.031>.
- [4] Y.H. Lee, Y.F. Lee, K.H. Chang, C.C. Hu, Synthesis of N-doped carbon nanosheets from collagen for electrochemical energy storage/conversion systems, *Electrochem. Commun.* 13 (2011) 50–53, <https://doi.org/10.1016/j.elecom.2010.11.010>.
- [5] Q. Wang, R. Yan Zhang, Y. Wu, H. Zhu, J. Zhang, M. Du, M. Zhang, L. Wang, X. Zhang, X. Liang, Silk-derived graphene-like carbon with high electrocatalytic activity for oxygen reduction reaction, *RSC Adv.* 6 (2016) 34219–34224, <https://doi.org/10.1039/C6RA07075B>.
- [6] B. Boury, S. Plumejeau, Metal oxides and polysaccharides: an efficient hybrid association for materials chemistry, *Green Chem.* 17 (2014) 72–88, <https://doi.org/10.1039/C4GC00957F>.
- [7] E. Senoz, J.F. Stanzione, K.H. Reno, R.P. Wool, M.E.N. Miller, Pyrolyzed chicken feather fibers for biobased composite reinforcement, *J. Appl. Polym. Sci.* 128 (2013) 983–989, <https://doi.org/10.1002/app.38163>.
- [8] E. Senoz, R.P. Wool, Microporous carbon-nitrogen fibers from keratin fibers by pyrolysis, *J. Appl. Polym. Sci.* 28 (2010) 1752–1765, <https://doi.org/10.1002/app.2010.1002.app.281752>.
- [9] I. Petrenko, A.P. Summers, P. Simon, S. Żóltowska-Aksamitowska, M. Motylenko, C. Schimpf, D. Rafaja, F. Roth, K. Kummer, E. Brendler, O.S. Pokrovsky, R. Galli, M. Wysokowski, H. Meissner, E. Niederschlag, Y. Joseph, S. Molodtsov, A. Ereskovsky, V. Sivkov, S. Nekipelov, O. Petrova, O. Volkova, M. Bertau, M. Kraft, A. Rogalev, M. Kopani, T. Jesionowski, H. Ehrlich, Extreme biomimetics: preservation of molecular detail in centimeter-scale samples of biological meshes laid down by sponges, *Sci. Adv.* 5 (2019) 1–12, <https://doi.org/10.1126/sciadv.aax2805>.
- [10] T. Szatkowski, K. Kocopyński, M. Motylenko, H. Borrmann, B. Mania, M. Graś, G. Lota, V.V. Bazhenov, D. Rafaja, F. Roth, J. Weise, E. Langer, M. Wysokowski, S. Żóltowska-Aksamitowska, I. Petrenko, S.L. Molodtsov, J. Hubáľková, C.

- G. Aneziris, Y. Joseph, A.L. Stelling, H. Ehrlich, T. Jesionowski, Extreme biomimetics: a carbonized 3D spongin scaffold as a novel support for nanostructured manganese oxide(IV) and its electrochemical applications, *Nano Res* 11 (2018) 4199–4214, <https://doi.org/10.1007/s12274-018-2008-x>.
- [11] L.-S. Zhang, X.-Q. Liang, W.-G. Song, Z.-Y. Wu, Identification of the nitrogen species on N-doped graphene layers and Pt/NG composite catalyst for direct methanol fuel cell, *Phys. Chem. Chem. Phys.* 12 (2010) 12055–12059, <https://doi.org/10.1039/c0cp00789g>.
- [12] S. Plumejeau, J.G. Alauzun, B. Boury, Hybrid metal oxide@biopolymer materials precursors of metal oxides and metal oxide-carbon composites, *J. Ceram. Soc. Japan*. 123 (2015) 695–708, <https://doi.org/10.2109/jcersj2.123.695>.
- [13] H. Ehrlich, M. Wysokowski, S. Żóltowska-Aksamitowska, I. Petrenko, T. Jesionowski, Collagens of poriferan origin, *Mar. Drugs* 16 (2018) 1–21, <https://doi.org/10.3390/md16030079>.
- [14] T. Jesionowski, M. Norman, S. Żóltowska-Aksamitowska, I. Petrenko, Y. Joseph, H. Ehrlich, Marine spongin: naturally prefabricated 3D scaffold-based biomaterial, *Mar. Drugs* 16 (2018) 1–23, <https://doi.org/10.3390/md16030088>.
- [15] P.R. Salgado, V.C. Schmidt, S.E. Molina Ortiz, A.N. Mauri, J.B. Laurindo, Biodegradable foams based on cassava starch, sunflower proteins and cellulose fibers obtained by a baking process, *J. Food Eng.* 85 (2008) 435–443, <https://doi.org/10.1016/j.jfoodeng.2007.08.005>.
- [16] G.S. Dhaliwal, S. Anandan, K. Chandrashekhar, N. Dudenhoefler, P. Nam, Fabrication and testing of soy-based polyurethane foam for insulation and structural applications, *J. Polym. Environ.* 27 (2019) 1897–1907, <https://doi.org/10.1007/s10924-019-01477-0>.
- [17] T.O.J. Blomfeldt, F. Nilsson, T. Holgate, J. Xu, E. Johansson, M.S. Hedenqvist, Thermal conductivity and combustion properties of wheat gluten foams, *ACS Appl. Mater. Interfaces* 4 (2012) 1629–1635, <https://doi.org/10.1021/am2017877>.
- [18] D. Istrate, C. Popescu, M. Möller, Non-isothermal kinetics of hard α -keratin thermal denaturation, *Macromol. Biosci.* 9 (2009) 805–812, <https://doi.org/10.1002/mabi.200800344>.
- [19] C.A. Miles, Kinetics of collagen denaturation in mammalian lens capsules studied by differential scanning calorimetry, *Int. J. Biol. Macromol.* 15 (1993) 265–271, [https://doi.org/10.1016/0141-8130\(93\)90025-H](https://doi.org/10.1016/0141-8130(93)90025-H).
- [20] C.A. Miles, T.V. Burjanadze, A.J. Bailey, The kinetics of the thermal denaturation of collagen in unrestrained rat tail tendon determined by differential scanning calorimetry, *J. Mol. Biol.* 245 (1995) 437–446, <https://doi.org/10.1006/jmbi.1994.0035>.
- [21] S. Vyazovkin, A.K. Burnham, J.M. Criado, L.A. Pérez-Maqueda, C. Popescu, N. Sbirrazzuoli, ICTAC Kinetics Committee recommendations for performing kinetic computations on thermal analysis data, *Thermochim. Acta* 520 (2011) 1–19, <https://doi.org/10.1016/j.tca.2011.03.034>.
- [22] S. Vyazovkin, Kinetic concepts of thermally stimulated reactions in solids: a view from a historical perspective, *Int. Rev. Phys. Chem.* 19 (2000) 45–60, <https://doi.org/10.1080/014423500229855>.
- [23] J. Sestak, V. Stava, W. Wendlandt, The study of heterogeneous processes by thermal analysis, *Thermochim. Acta* 7 (1973) 333–356.
- [24] T. Ozawa, Kinetic analysis of derivative curves in thermal analysis, *J. Therm. Anal.* 2 (1970) 301–324, <https://doi.org/10.1007/BF01911411>.
- [25] L.J. Goldfarb, R. McGuchan, A.C. Meeks, Kinetic Analysis of Thermogravimetry, Technical Report AFML-TR-68-181, Part II, Air Force Materials Laboratory Air Force, Systems Command Wright-Patterson Air Force Base, Ohio, 1968.
- [26] A.W. Coats, J.P. Redfern, Kinetic parameters from thermogravimetric data, *Science* 201 (1964) 68–69.
- [27] A.A.K. Galwey, M.E. Brown, Kinetic models for solid-state reactions, in: A. K. Galwey, M.E. Brown (Eds.), *Thermal Decomposition of Ionic Solids*, Elsevier, Amsterdam, 1998, pp. 75–139, <https://doi.org/10.16309/j.cnki.issn.1007-1776.2003.03.004>.
- [28] C.D. Doyle, Kinetic analysis of thermogravimetric data, *J. Appl. Polym. Sci.* 5 (1961) 285–292, <https://doi.org/10.1021/j100853a022>.
- [29] S. Vyazovkin, C.A. Wight, Model-free and model-fitting approaches to kinetic analysis of isothermal and nonisothermal data, *Thermochim. Acta* 340 (1999) 53–68, [https://doi.org/10.1016/S0040-6031\(99\)00253-1](https://doi.org/10.1016/S0040-6031(99)00253-1).
- [30] H.L. Friedman, Kinetics of thermal degradation of char-forming plastics from thermogravimetry. Application to a phenolic plastic, *J. Polym. Sci. Part C Polym. Symp.* 6 (1964) 183–195, <https://doi.org/10.1002/polc.5070060121>.
- [31] L.T. Vlaev, I.G. Markovska, L.A. Lyubchev, Non-isothermal kinetics of pyrolysis of rice husk, *Thermochim. Acta* 406 (2003) 1–7, [https://doi.org/10.1016/S0040-6031\(03\)00222-3](https://doi.org/10.1016/S0040-6031(03)00222-3).
- [32] E. Senoz, R.P. Wool, C.W.J. McChalicher, C.K. Hong, Physical and chemical changes in feather keratin during pyrolysis, *Polym. Degrad. Stabil.* 97 (2012) 297–307, <https://doi.org/10.1016/j.polymdegradstab.2011.12.018>.
- [33] M. Brebu, I. Spiridon, Thermal degradation of keratin waste, *J. Anal. Appl. Pyrolysis* 91 (2011) 288–295, <https://doi.org/10.1016/j.jaap.2011.03.003>.
- [34] R. Wetzel, L.J. Perry, W.A. Baase, W.J. Becktel, Disulfide bonds and thermal stability in T4 lysozyme, *Proc. Natl. Acad. Sci. U.S.A.* 85 (1988) 401–405, <https://doi.org/10.1073/pnas.85.2.401>.
- [35] S. Kasap, J. Málek, R. Svoboda, S. Kasap, P. Capper, Thermal properties and thermal analysis: fundamentals, experimental techniques and applications, in: *Springer Handbook of Electronic and Photonic Materials*, Springer Handbooks. Springer, Cham, 2017, https://doi.org/10.1007/978-3-319-48933-9_19.H.
- [36] Moussout, H. Ahlafi, M. Aazza, M. Bourakhouadar, Kinetics and mechanism of the thermal degradation of biopolymers chitin and chitosan using thermogravimetric analysis, *Polym. Degrad. Stab.* 130 (2016) 1–9, doi:10.1016/j.polymdegradstab.2016.05.016.
- [37] J.H. Flynn, The “temperature integral” - its use and abuse, *Thermochim. Acta* 300 (1997) 83–92, [https://doi.org/10.1016/S0040-6031\(97\)00046-4](https://doi.org/10.1016/S0040-6031(97)00046-4).
- [38] H. Moussout, H. Ahlafi, M. Aazza, C. Sekkate, Kinetic and mechanism studies of the isothermal degradation of local chitin, chitosan and its biocomposite bentonite/chitosan, *Cellulose* 25 (2018) 5593–5609, <https://doi.org/10.1007/s10570-018-1999-5>.
- [39] R.K. Mishra, K. Mohanty, Pyrolysis kinetics and thermal behavior of waste sawdust biomass using thermogravimetric analysis, *Bioresour. Technol.* 251 (2018) 63–74, <https://doi.org/10.1016/j.biortech.2017.12.029>.
- [40] P.E. Sánchez-Jiménez, L.A. Pérez-Maqueda, A. Perejón, J. Pascual-Cosp, M. Benítez-Guerrero, J.M. Criado, An improved model for the kinetic description of the thermal degradation of cellulose, *Cellulose* 18 (2011) 1487–1498, <https://doi.org/10.1007/s10570-011-9602-3>.
- [41] R.R. Gil, R.P. Girón, M.S. Lozano, B. Ruiz, E. Fuente, Pyrolysis of biocollagenic wastes of vegetable tanning. Optimization and kinetic study, *J. Anal. Appl. Pyrolysis* 98 (2012) 129–136, <https://doi.org/10.1016/j.jaap.2012.08.010>.
- [42] J.C. Bischof, X. He, Thermal stability of proteins, *Ann. N. Y. Acad. Sci.* 1066 (2005) 12–33, <https://doi.org/10.1196/annals.1363.003>.
- [43] S. Tiptipakorn, S. Rimsudit, P. Suwanmala, K. Hemvichian, Thermal degradation kinetics of polyurethane/polybenzoxazine alloys, *Adv. Mater. Res.* 214 (2011) 439–443, www.scientific.net/AMR.214.439.
- [44] P. Król, K. Pielichowska, Ł. Byczyński, Thermal degradation kinetics of polyurethane-siloxane anionomers, *Thermochim. Acta* 507–508 (2010) 91–98, <https://doi.org/10.1016/j.tca.2010.05.005>.